

256×8 SPAD Array With 256 Column TDCs for a Line Profiling Laser Radar

Pekka Keränen^{IP} and Juha Kostamovaara^{IP}, *Senior Member, IEEE*

Abstract—A receiver circuit for pulsed time-of-flight line profiling laser radar has been designed in 0.35 μm CMOS technology. The receiver consists of a line detector array with 256×8 SPADs with a pitch of 41.6 μm . The diameter of the SPAD's active area is 25.6 μm , which gives a fill factor of 0.35. Each column has 8 SPADs and a TDC with a range and resolution of 640 ns and 20 ps, respectively. The TDCs are based on the Nutt interpolation method where cyclic converters are utilized as fine converters. A compact demonstrator system has been built with a horizontal FOV of about 37°, which gives a column-wise angular resolution of about 0.15°. This solid-state system uses a pulsed laser diode with cylindrical transmitter optics to illuminate the full FOV of the receiver with a single laser pulse. The system can measure distances up to 30 m @ 28 fps with an accuracy and precision of few millimeters in typical indoor lighting conditions. Outdoors, in direct sunlight conditions, the measurement range is decreased to 5 m. Outdoor range, however, can be increased if frame rate is lowered and more laser shots are accumulated per frame.

Index Terms—Time-to-digital converter (TDC), single photon avalanche diode (SPAD), time-of-flight (ToF), light detection and ranging (LiDAR).

I. INTRODUCTION

PULSED time-of-flight (TOF) laser radar operates on the principle of sending a high power (>10W) and short (<5ns) laser pulse towards the target, and then measuring the time-of-flight by measuring the time difference between the transmitted pulse and the reflected echo pulse [1]–[4]. Since the velocity of light is relatively constant, the distance to the target can be calculated based on the measured transit time. These techniques have important advantages compared to other optical time-of-light methods, e.g. to the measurement of the phase difference between the transmitted continuous-wave (CW) optical signal and the reflected echo. For a pulsed TOF system, the non-ambiguous measurement range is limited basically by the pulsing rate of the transmitter and can thus be very long (i.e. 100m with 1MHz) whereas in the CW phase comparison techniques there is a trade-of between the non-ambiguous

measurement range and measurement precision [5]–[9]. Also, the pulsed TOF method allows the detection of multiple return echoes, which is an issue for the CW method however, and which may easily happen in practice when several targets at different distances are under the illumination of the measurement beam.

Pulsed TOF laser radar techniques have traditionally been used in applications where a single measurement axis is enough, e.g. in the measurement of level heights in silos and containers, in geodesy and civil engineering and in traffic control. Recently, however, new applications have been suggested within the fields of robotics, man-machine-communication, traffic, smart home, gesture control, security and small vehicle guidance devices (e.g. unmanned aerial vehicles, UAVs), for example [10], [11]. The distinct difference between the traditional and new applications is that in most of the new applications the laser radar system should be able to measure not only along a single direction but to several directions simultaneously. In fact, in most cases, a system capable to produce a 2-D or 3-D range image about its environment within a certain field-of-view (FOV) is required. Traditionally, 2-D or 3-D range imagers have been realized by mechanically spinning the radar or a mirror, or by a combination of both techniques [12]. These instruments are in many cases accurate and adequate for many applications, but also quite complex with high power consumption and relatively high costs. Thus, in most of the new applications, a solid-state realization without any moving parts would be preferred. That would also pave the way towards the realization of a range imager in miniature size and low costs.

Traditional pulsed TOF laser radar are based on linear detection techniques, i.e. the optical signal is detected with a linear photo detector, in most cases with an avalanche photo diode (APD), and then processed with linear receiver techniques. This approach, however, has limitations with regards to the spatial resolution in 2-D or 3-D range imaging due to limited supply of dense APD arrays. Also, the complexity of the receiver electronics and limitations with regards to the laser pulse power are obviously issues.

Another pulsed TOF measurement approach would be the utilization of single photon detection techniques (SPAD) in the receiver [13], [14]. As is well known, a SPAD detector can be realized in conventional CMOS technology as a high density 1-D or 2-D array with relatively good performance characteristics, and thus these techniques have found applications in ranging and optical spectroscopy, see for example [15]–[21] and references therein. The photon detection efficiency is

Manuscript received March 1, 2019; revised May 16, 2019; accepted June 7, 2019. Date of publication June 28, 2019; date of current version October 30, 2019. This work was supported in part by the Academy of Finland, Centre of Excellence in Laser Scanning Research, under Contract 307362 and Contract 317144, and in part by the Business Finland under Contract 2773/31/2015. This paper was recommended by Associate Editor H. Zhang. (*Corresponding author: Pekka Keränen.*)

The authors are with the Circuits and Systems Research Unit, Faculty of Information Technology and Electrical Engineering, University of Oulu, 90014 Oulu, Finland (e-mail: pekka.keranen@oulu.fi; juha.kostamovaara@oulu.fi).

Color versions of one or more of the figures in this article are available online at <http://ieeexplore.ieee.org>.

Digital Object Identifier 10.1109/TCSI.2019.2923263

typically <4% at the wavelength of high-power pulsed lasers (>800nm), but even in this case, only a small number of photons (~50) is enough to introduce the breakdown in a SPAD element with high probability. This is considerably less than in the conventional linear detection techniques [22]. The jitter of the avalanche breakdown is around ~100ps, which indicates the possibility for high single-shot precision. Also, the use of standard CMOS technology makes it possible to combine the needed electronics, e.g. time-to-digital converters (TDC), on the same semiconductor die. A remarkable fact is that the use of SPADs as photodetectors enables one to skip the analog receiver completely since the detector element itself can produce a digital-like output signal for the time interval measurements. Thus, also the serious issue of cross-talk which is typically present when high speed, low noise amplifiers are used in the neighborhood of high current slew-rate drivers (the laser transmitter) is avoided. In fact, if short and high power laser pulses are being used together with SPAD detectors, the laser radar, which in the traditional sense is an analogue system, is transformed into a digital radar, i.e. sending impulse like pulses and digitally detecting the photons within the pulse envelope instead of the pulse envelope itself. The way how background radiation (Sun, for example) affects the measurement, however, changes. In the linear system it merely adds a shot noise component into the equivalent input current noise of the receiver channel and thus signal-to-noise ratio for its part in the detection is decreased. In the single photon detection based system, background radiation produces random detections not distinguishable from the detections produced by the photons reflected from the target. These random background detections may even block the detections from the target if the background level is high enough. Thus, a single measurement is not enough for a reliable distance estimation but instead a number of repeated measurements is required. Histogram analysis of the results based on several separate measurements is typically needed.

Since random counts induced by the detector itself (dark counts), as well as the background illumination, constitute the noise of a SPAD based receiver, it is intuitively appealing to use short and energetic laser pulses for the distance measurement. Since the amount of photons in a pulse is proportional to the total energy of the pulse, a higher amplitude(power), assuming constant pulse energy and operation in the single photon detection mode, gives also a higher probability for the detection at the receiver. As a result, fewer transmitted pulses are needed for a certain number of valid detections from the target. Thus, also the total number of random false detections is lower, resulting in shorter measurement time. In addition to the improved signal-to-noise ratio (SNR), also the precision of the measurement is improved due to the shorter pulse.

Motivated by the above thoughts, we have developed a solid-state 2-D line profiler utilizing the pulsed TOF technique. The system, with a size of a typical CMOS camera, uses a laser diode transmitter with a pulse energy and width of ~1nJ-2nJ/100ps-500ps, respectively. The custom designed quantum well laser diode with a stripe width/cavity length of 30µm/3mm operates @ 810nm and has been specifically

designed for the generation of short and energetic optical pulses [23], [24].

The receiver consists of a SPAD array with 256×8 elements and 256 high performance time-to-digital converters, which all are located on a single CMOS chip. The results are collected with an FPGA, which also connects the device to a PC through USB. Power for the whole system is also provided through USB. The horizontal field of view is ~37°, and it can produce line profiles from non-cooperative targets with a spatial resolution of ~0.15° at a typical distance of 20m with a frame rate of >20fr/sec in a background illumination of 10klux. In this paper, the main focus is in the description of the receiver part of the system (the CMOS receiver IC), but in order to validate the operation of the receiver, also system level measurement results are presented.

II. 2-D LINE PROFILER ARCHITECTURE AND SYSTEM ANALYSIS

A. System Concept

In the proposed solid-state 2-D range imaging concept, a horizontal (or vertical) laser stripe illuminates the target within the field-of-view (FOV) of the receiver. In this particular design, the width of the laser stripe is about 0.3° x 37° and it is produced with cylindrical optics from the output of the laser diode. The pulse rate is about 140kHz, while the pulse energy and pulse width(FWHM) are ~1nJ-2nJ and ~100ps-500ps, depending on the drive strength of the laser diode. The receiver circuit consists of 8 lines of 256 SPAD elements and it is located on the focal plane of the receiver optics. Thus, the laser stripe on the target produces a line image on the detector surface. The optics are dimensioned in such a way that the 37° FOV of the system is fully covered with the 256 SPADs of the line array. Each of the SPADs measures actually into a certain “angular direction”, i.e. the system FOV is divided into vertical slices determined by the number of the SPAD elements on the line, see Fig. 1a. In this case, the lateral dimension of the measurement spot corresponding with a single detector element varies of course as a function of distance, which however is acceptable as long as the desired spatial resolution is achieved. The important consequence is that the receiver optics needs to be focused only once (basically for infinity) and not along the changing distance of the target. In the developed system, the vertical thickness of the line image on the detector surface is ~80µm. Thus, the line image covers approximately two SPAD lines with a SPAD pitch of 41.6µm. However, due to the biaxial optics(receiver below transmitter) the line image moves vertically on the detector surface if the target distance changes. For this reason, the detector uses 8 lines of SPADs, out of which any combination can be connected to the column-wise TDC elements. The raw distance measurement data produced by the 2-D range imager system is a set of column-wise histograms which each include the number of hits as a function of measured time interval with the selected number of sent laser pulses.

A typical potential applications for this kind of a 2-D range imager is a safety curtain in an excavator or in another machine where the engine driver has a restricted view around the machine (Fig. 1b). Another typical use for a line profile is

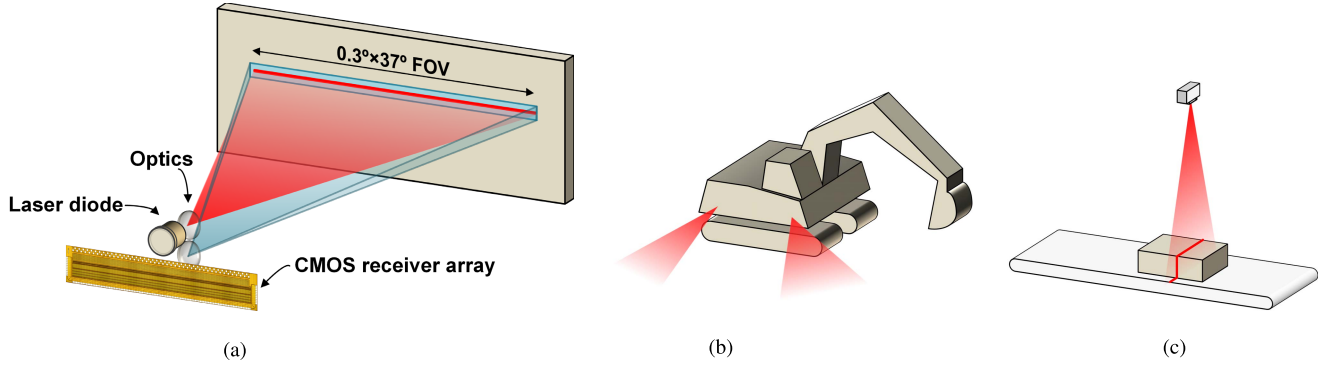


Fig. 1. Line profile laser radar concept and potential applications as an example.

in recording the 3-D profile of the material transported with a conveyor belt (Fig. 1c). In the latter application, the running conveyor belt “automatically” produces the movement of the measurement object perpendicularly to the 2-D measurement line, and thus a full 3-D range image of the object is eventually produced.

The advantage of a line sensor is that the receiver complexity is considerably relaxed when one of the dimensions, horizontal or vertical, can be discarded. The number of TDCs required by a line sensor becomes more feasible than in a full 3-D range imager, and therefore, also area constraints per TDC are more relaxed. On the illumination side, the optical power can be concentrated in one dimension, thus the available optical power per SPAD can be high, which makes it possible for the line sensor to measure relatively long distances with high frame rates.

B. Radiometric Analysis

When the receiver array consists of N_{spad} SPADs with a fill factor of FF , and when it is assumed that the FOV of the receiver array matches the illumination beam (with uniform radiance and total pulse energy of Q_{lsr}), the transmitted radiant energy per SPAD is $FF Q_{lsr} / N_{spad}$.

When the optical pulse is transmitted and reflects from a diffuse and flat target at a distance R , the average number of reflected photons received by a single SPAD can be expressed as [25]

$$N_{sig}(R) = Q_{lsr} \frac{\lambda}{hc} \frac{FF}{N_{spad}} \left(\frac{d_r}{2} \right)^2 \frac{\cos(\theta)}{R^2} \rho_t \quad (1)$$

where N_{spad} is the number of SPADs in the receiver array, FF is the fill-factor of the SPAD array, λ is the wavelength of the optical pulse, h is Planck’s constant, c is the speed of light, d_r is the diameter of the receiver aperture, θ is the angle of incidence between the laser beam and the surface normal and ρ_t is the reflection coefficient of the target surface.

When the target is also illuminated by background light with an irradiance of $E_e(\lambda)$, the average number of background photons received in a time window of Δt_w is

$$N_{bg}(\Delta t_w) = E_e(\lambda) \frac{\lambda}{hc} \Delta \lambda_{bw} \Delta t_w \left(\frac{d_r}{2} \right)^2 \pi \left(\frac{d_{spad}}{2F} \right)^2 \cos(\phi) \rho_t \quad (2)$$

where $\Delta \lambda_{bw}$ is the optical bandwidth of the receiver, d_{spad} is the effective diameter of a single SPAD, F is the focal length of the receiver and ϕ is the angle of incidence between the background light and the surface normal.

If the SPAD is activated (recharged) at the same time when the laser pulse is transmitted, the probability to detect a reflected signal photon or a background photon during a time window of Δt_{lsr} (i.e. the length of the illumination pulse) from a distance R is roughly given by

$$P_{s+bg}(R) = e^{-PDP N_{bg} \left(\frac{2R}{c} \right)} \left(1 - e^{-PDP (N_{bg}(\Delta t_{lsr}) + N_{sig}(R))} \right) \quad (3)$$

where PDP is the photon detection probability of the SPAD.

In the absence of signal, the probability to detect background photon is

$$P_{bg}(R) = e^{-PDP N_{bg} \left(\frac{2R}{c} \right)} \left(1 - e^{-PDP N_{bg}(\Delta t_{lsr})} \right) \quad (4)$$

The exponential terms arise from the fact that the SPAD operates in a single-detection mode, i.e. after the first photon detection, all subsequent photons are lost until the SPAD is recharged again when the next laser pulse is transmitted. In order to detect a signal from a distance R , it is required that the SPAD has not already detected a background photon before the arrival of reflected signal photons. Reflected signal photons take $2R/c$ seconds to arrive from the target, thus the signal detection probability is reduced by the term $e^{-PDP N_{bg} \left(\frac{2R}{c} \right)}$, which is the probability that no background detection has occurred before the signal photons are received.

When the measurement is repeated n times (i.e. n laser pulses are transmitted), the number of accumulated detections within the time window of the reflected laser pulse (Δt_{lsr}) is assumed to be binomially distributed with a mean and variance of

$$\begin{aligned} \mu_{s+bg}(R) &= n P_{s+bg}(R) & \sigma_{s+bg}(R) &\approx \sqrt{n P_{s+bg}(R)} \\ \mu_{bg}(R) &= n P_{bg}(R) & \sigma_{bg}(R) &\approx \sqrt{n P_{bg}(R)} \end{aligned} \quad (5)$$

where it is assumed that $P(R) \ll 1$.

Next we will derive an expression to approximate a threshold above which signal detections can be still distinguished from background detections. For simplicity, we assume that

the skewness of the binomially distributed detection count is negligible, and thus we approximate the detection counts within the time window of Δt_{lsr} with a normal distribution in order to derive the upper and lower limits for the detection counts.

In the presence of signal, the lower limit for the number of detections is estimated as $\mu_{s+bg}(R) - z\sigma_{s+bg}(R)$, where z is the quantile parameter of the standard normal distribution. For example, when $z = 2$ the detection count is higher than the lower limit with a probability of 0.975.

Similarly, in the absence of reflected signal, the upper limit for the number of detections is given by $\mu_{bg}(R) + z\sigma_{bg}(R)$. Thus, in order to reliably distinguish the reflected echo from the background, we require that in presence of signal, the lower limit for the detection count is larger than what the upper limit would be if only background is present.

$$\begin{aligned} \mu_{s+bg}(R) - z\sigma_{s+bg}(R) &> \mu_{bg}(R) + z\sigma_{bg}(R) \\ \Leftrightarrow nP_{s+bg}(R) - z\sqrt{nP_{s+bg}(R)} &> nP_{bg}(R) + z\sqrt{nP_{bg}(R)} \end{aligned}$$

Since $nP_{s+bg} \geq 0$, $nP_{bg} \geq 0$, $z \geq 0$, we arrive at

$$\sqrt{nP_{s+bg}(R)} > \sqrt{nP_{bg}(R)} + z \quad (6)$$

The quantile parameter z can typically range from 2 – 4 depending on how strong the signal is required to be in order to be detectable and distinguishable from background detections. In case of no background, the above equation becomes $nP_s(R) > z^2$, i.e. the average number of signal detections per frame is required to be higher than z^2 in order for the signal to be considered detectable.

The measurement range of the designed line profiler has been estimated by plugging (3) and (4) into (6) and numerically solving for R . The threshold parameter z was 2.5, angle of incidence was assumed to be zero, pulse energy 2nJ (i.e. ~ 8 pJ per receiver column), PDP is assumed to be 4%, the bandwidth of the optical filter is 20nm, the laser pulsing rate is 140kHz and the frame rate is 28, thus the result of 5000 laser shots are accumulated per frame. Fig. 2 shows a contour plot of measurement range against different background irradiance and reflection coefficient values.

It can be roughly estimated, that when the target is illuminated by direct sunlight, the background irradiance @ 810nm is in the range of $0.5 - 1 \text{ W}/(\text{m}^2 - \text{nm})$. When the target is located in a shade and indirectly illuminated by the sun, the background irradiance is roughly reduced by a factor of 10 and when the target is indirectly illuminated by typical indoor lighting conditions, the irradiance is reduced by another factor of 10. This high variability in background irradiance means that the maximum measurement range of the system (with the above pulse energy, pulsing rate and frame rate) is somewhere between 5m-30m depending on the background conditions.

C. Receiver Architecture and Circuit Details

The CMOS receiver chip consists of a 256×8 SPAD array with 256 TDCs (one for each column). A block diagram of the receiver architecture is shown in Fig. 3.

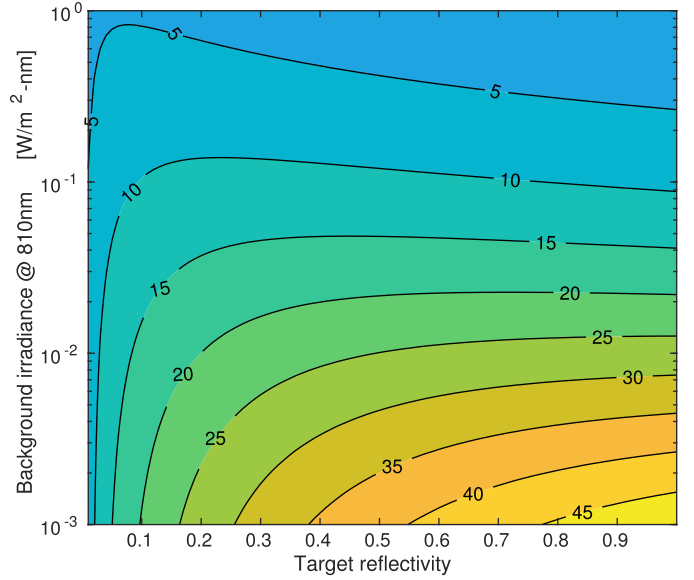


Fig. 2. Estimated maximum measurement range (28fps @ 140kHz pulse rate) of the line profiler vs. background irradiance and reflection coefficient.

The column TDCs are based on the Nutt interpolation method, where cyclic data conversion approach is used within the interpolators. In the Nutt interpolation method, an accurate reference clock counter is used as a coarse quantizer to measure the time interval. Picosecond level precision is provided by two fine quantizers (interpolators) that capture the arrival times of the *start* and the *stop* signals within the reference clock period. Because the *start* signal from the laser driver circuit is common to every TDC, a shared *start* interpolator is used for all the TDCs. Thus each TDC column consists of a reference clock counter and a *stop* interpolator as shown in Fig. 3.

The time measurement range and the nominal resolution of the TDC is 620ns and 20ps, respectively. The interpolators utilize delay line based PVT tolerant pulse width doublers to construct a cyclic data converter. A detailed description of the cyclic interpolators and the performance of the whole TDC array is provided in [26]. The performance of the TDCs has been measured to provide a single-shot precision of about 70ps, while the DNL and INL for the TDCs are $+0.3/ - 0.2$ LSBs and $+1.3/ - 1$ LSBs, respectively. The power consumption of a single TDC channel is about 1.2mW @ 100kHz conversion rate, however, most of the power is actually consumed in the read-out phase.

All the SPADs in the array have a common cathode as they are all placed in one large n-well. The anode consists of p+ active area surrounded by a p-well guard ring. The diameter of the active area is $25.6\mu\text{m}$ and the SPAD pitch is $41.6\mu\text{m}$, which gives a fill factor of about 0.35. Each column consists of 8 SPADs, since biaxial transmitter/receiver optics are used. The vertical location of the illumination beam on the sensor varies when the target distance varies. The amount of beam movement on the receiver sensor depends on the focal length and the physical distance between the transmitter and the receiver on the PCB, and on this design the beam movement

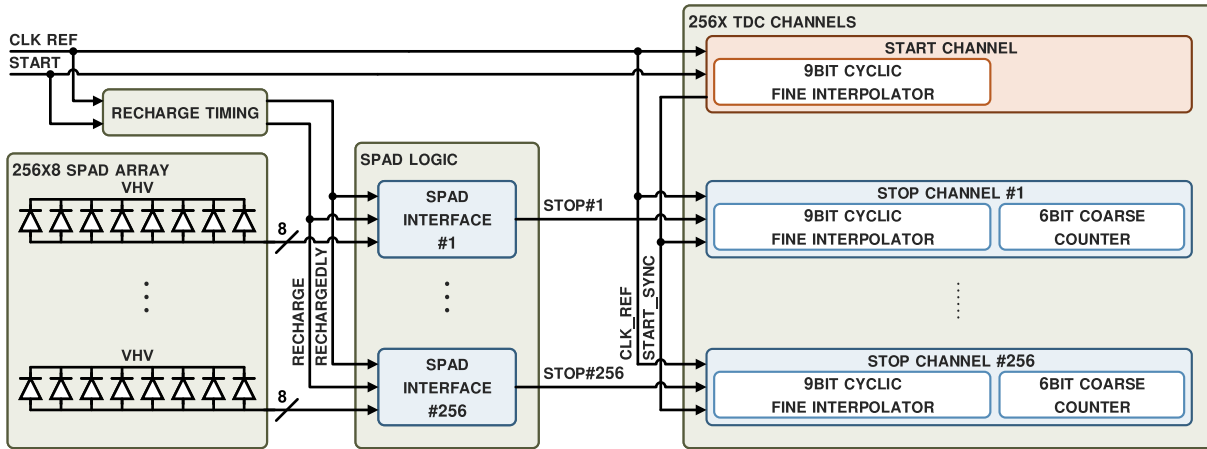


Fig. 3. Block diagram of the line profiler receiver chip.

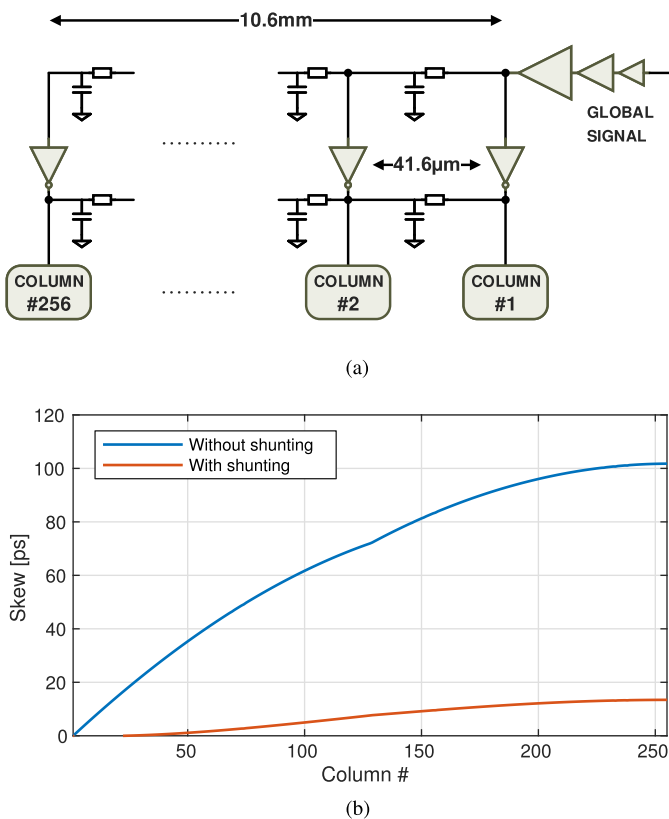


Fig. 4. Distribution of timing sensitive global signals. (a) Buffering of timing critical global signals with shunted column level buffers to deskew RC wire delays. (b) Post-layout simulated skew along the columns with and without column level shunting.

is about $350\mu\text{m}$ when the target distance is between 1m to infinity, which is covered by the 8 SPAD rows.

Another reason for having 8 SPADs in a single column, is that the receiver focus is typically set to infinity. The transmitter and receiver optics have been designed so that when the target is in focus, the received beam covers two of the eight SPADs. However, when the distance to target is less than few meters, the received optical power will spread on more than two SPADs.

No in-pixel electronics are used, but the anode voltage of each SPAD is sensed by an interface circuit located outside

of the SPAD array. In addition to sensing the breakdown, the interface circuit takes care of recharging, quenching and enabling/disabling the pixel. The SPAD recharge timing is controlled by a global timing circuit. The width of the recharge pulse, and the relative delay of the recharge pulse with respect to the TDC's *start* signal can be controlled. Thus, the SPADs are activated synchronously with respect to the TDC's *start* signal rather than allowing them to recharge randomly in "free-running" mode.

One of the goals with the receiver has been to minimize channel-to-channel timing differences in order to avoid channel-wise calibration. The receiver ic will unavoidably contain delays that require correction, but with careful design and proper architecture, we have tried to make all the 256 channels as uniform as possible when timing is considered. If the timing delays associated with all the channels is identical, a single offset correction term can be used to compensate all measurement channels. This offset correction is required in any case, since components external to the receiver chip will always introduce some additional delays which needs to be compensated. For example, a delay difference of 70ps between transmitting the laser pulse and starting the time interval measurement on the receiver ic is equivalent to an offset error of 1cm.

In order to realize a uniform receiver system, the TDCs, for example, use a stable external reference oscillator to ensure identical LSB size in each channel, which minimizes any gain differences between the channels. Besides the TDCs, the top-level of the receiver architecture also requires careful design, since the receiver has several global timing signals, such as the reference clock, the *start* signal and the *recharge* signals, that should be received by each column with as little skew as possible in order to avoid offset variations between the channels. Binary tree buffering and balanced distribution of signals to all the columns would be ideal, however the placement of buffers and matching of wire lengths and parasitics is difficult. Instead of a balanced binary tree, a simple buffering approach shown in Fig. 4a was used. First a tapered buffer drives the global signal across the columns, and then column level buffers with shunted outputs are used to deskew the signal. Based on post-layout simulations with

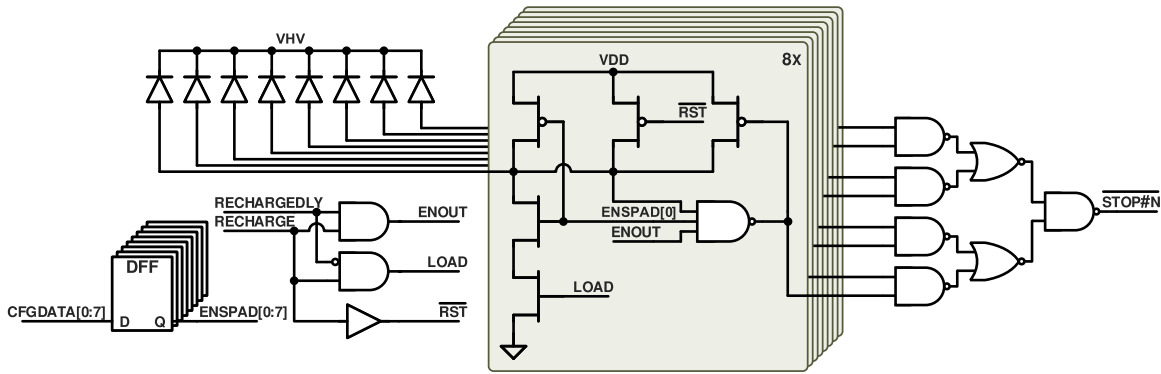


Fig. 5. Interface circuit for a column of SPADs.

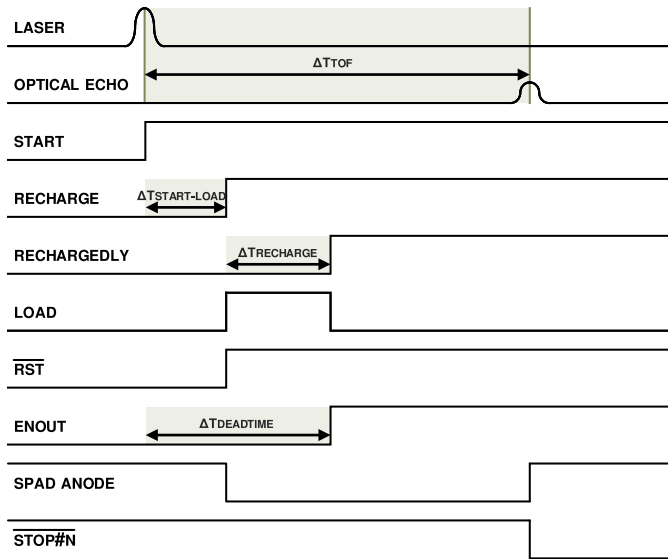


Fig. 6. Timing diagram illustrating the operating principle of the receiver.

extracted RC parasitics, the shunting improves the timing skew between the first and the last column from around 100ps to 10ps as shown in Fig. 4b, which depicts the difference of signal arrival times in the different columns with respect to the first column in the array. The average delay from the input of the tapered buffer to the column inputs is about 790ps. Most of this delay is caused by the tapered buffer and the distributed RC load. Without shunting on the second level of buffering, the average delay at the column inputs is about 730ps, thus the shunting increases the average delay by about 60ps, but reduces the skew between columns by 90ps.

Fig. 5 shows the SPAD interface logic for a single column. A timing diagram shown in Fig. 6 illustrates a single measurement sequence and the operating principle of the profiler.

Each column has a set of DFFs, which can be loaded with configuration data, $CFGDATA[0:7]$, in order to select active pixels within the column. The DFF output, $ENSPAD[0:7]$, controls the interface output through a NAND gate and also drives a PMOS/NMOS pair which is used to disable recharging and to pull the SPAD anode to VDD in case the pixel is

disabled. Thus each SPAD can be independently turned-off in case the pixel is defective or if the column-wise background detection rate needs to be suppressed by disabling pixels that are unnecessary for the detection of the reflected pulse.

All the SPADs in the array share a common *recharge* signal. The *recharge* signal is derived from the external *start* signal that starts the time interval measurement. The external *start* signal, in turn, is synchronous with the optical laser pulse and is derived by sensing the current pulse through the laser diode in order to minimize jitter with respect to the optical output pulse.

A global configurable delay circuit can be used to delay the *recharge* signal with respect to the *start* signal. Furthermore, a delayed version of the *recharge* signal, *rechargedly*, is also generated. Both signals are routed to every SPAD interface circuit and the time difference between the *recharge* and *rechargedly* signals determines the length of the *load* pulse that biases the SPAD above its breakdown voltage and then leaves the anode floating.

As shown in Fig. 6, these configurable signal delays allows the adjustment of the *start-to-load* delay and the adjustment of the *load* pulse length. The *start-to-load* delay can be configured with a step of 20ns. Thus, the activation of the SPADs can be delayed with respect to the transmitted optical pulse, and can be used, for example, to scan through the measurement range in case of high ambient light conditions, which could otherwise block the receiver from detecting echoes from targets far away. Although the deadtime induced by the adjustable *start-to-load* delay is desired for background rejection, the finite length of the *load* pulse also introduces deadtime that can limit the minimum distance which can be measured by the device if the delay is not compensated externally. SPAD breakdowns triggered during the load pulse will not be sensed by the TDC until the load pulse ends, and thus the collected histograms will show a pile-up of results in the first few bins.

At the same time when the *load* signal leaves the SPAD anode floating, *enout* signal goes high, which enables a NAND gate to detect a low-to-high transition at the SPAD anode. When a breakdown is detected, the output of the NAND gate goes low and a positive feedback loop formed by the NAND and a PMOS pull-up resets the anode voltage to VDD.

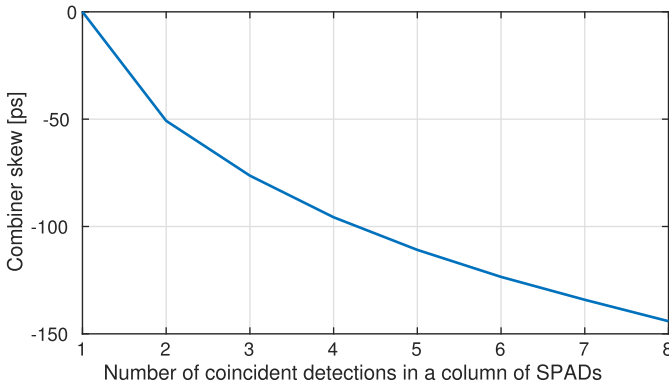


Fig. 7. Simulated timing skew of the NAND/NOR combiner, when more than one SPAD is triggered at the same time.

After all TDC channels have completed a measurement, or if a timeout occurs (i.e. the time interval exceeds the TDC range), a global reset signal is applied that resets all SPADs until the next laser pulse is transmitted.

All outputs from the eight SPAD interface circuits are combined by a NAND/NOR network so that the first SPAD to trigger also triggers the TDC. However, when several SPADs trigger at the same time, the delay of the combining network decreases since the drive strength of a NAND/NOR gate increases when both inputs go low/high simultaneously. This can lead to nonlinearity, if for example, the echo signal is strong enough to always trigger more than one SPAD simultaneously. Jitter, or deviation of ToF results, can be expected if the amount of triggered SPADs varies between laser shots.

Fig. 7 shows the simulated skew of the combiner, when one or more SPADs trigger simultaneously. Simulated worst case delay skew of about ~ 150 ps occurs if all eight SPADs trigger exactly at the same time. However, in practice, the probability of several SPADs to trigger exactly at the same time is very small. Furthermore, the received line profile beam only covers two of the eight SPADs at a time when the target is in focus, thus the worst case skew due to the combiner should be around 50ps at maximum.

III. EXPERIMENTAL RESULTS

A photomicrograph of the designed receiver circuit is shown in Fig. 8. The chip dimensions are $11.6\text{mm} \times 2.1\text{mm}$ (with pad ring). About 70% of the core area is taken by the TDCs, SPAD interface logic and read-out logic.

A line profiling 2D laser radar was constructed using the designed receiver. Fig. 9a shows a photograph of the PCB with the custom laser diode [23], [24] and the receiver IC. The complete USB powered line profiler system with optomechanics is shown in Fig. 9b. A OpalKelly XEM-7310 FPGA development board is used for control and handling data transfers through USB to a PC.

ToF results were estimated by collecting and processing histograms of raw time interval measurement results. The SPADs are charged above breakdown voltage at the same time when the laser pulse is transmitted. Because only one

SPAD triggering can be detected per laser shot, the histograms are distorted when the photon rate impinging the SPAD is very high. For example, in high ambient light conditions, the captured raw histogram is not flat (i.e. uniformly distributed), but instead the results follow exponential distribution as shown in Eqn. (4). Because of this, the histograms are first normalized with an approximation of the maximum-likelihood estimator for the true photon detection rate presented in [27]. The compensated number of detections in a histogram bin i can be calculated as

$$n'_i = \frac{N n_i}{N - \sum_{j=0}^{i-1} n_j}, \quad (7)$$

where N is the total number of laser shots and n_i is the number of detections in a bin i . After this, the normalized histogram is filtered with a triangular function by convolution. The width of the triangular filter is approximately equal to the width of the optical laser pulse. The peak value and the corresponding time interval is then located in the filtered histogram. In order to verify that the peak is a real echo from an object, ambient light level is also approximated from the histogram. A very coarse approximation for the ambient light level is given by simply calculating the average number of hits in all of the compensated histogram bins. This average is assumed to give an approximation for the term μ_{bg} in Eqn. (6). Before making a comparison with the peak value, a noise margin, i.e., the term $z\sigma_{bg}$ in Eqn. (6) is also approximated and added to the background estimate. This noise margin term depends on the number of laser shots, background estimate, filter width and the above compensation. After this, the peak value is compared to the background estimate plus noise margin, and a decision is made if the peak is considered to be a real echo.

The output characteristics of the used laser diode is shown in Fig. 10, which shows the transmitted optical transient with various drive strengths measured with an IR photodetector and a high speed oscilloscope. The maximum pulse energy is roughly about 2nJ while the peak power is almost 8W.

Fig. 11 shows a normalized histogram of a received echo from a white wall @ 3m distance. For reference, the transmitted optical pulse transient is also shown. The normalized histogram matches the real optical pulse quite well, with only the width being slightly widened.

Fig. 12 shows histograms for different levels of SPAD reverse bias. Too low reverse bias causes skew and increases the width of the histogram, which in turn decreases the accuracy and precision when distance measurement is considered.

SPAD dark count rate (DCR) was also measured with various reverse bias voltages. Fig. 13 shows the cumulative probability distribution of DCR of the SPAD array for different reverse bias voltages. The median DCR is about 40kHz when the SPAD voltage is about 22.5V. With this particular receiver system, this level of DCR is comparable to conditions, where a target with a reflectivity of 0.5 is illuminated by ambient light with an irradiance of $10^{-3} \text{W/m}^2 - \text{nm}$, which very roughly corresponds to very weak indoor light conditions.

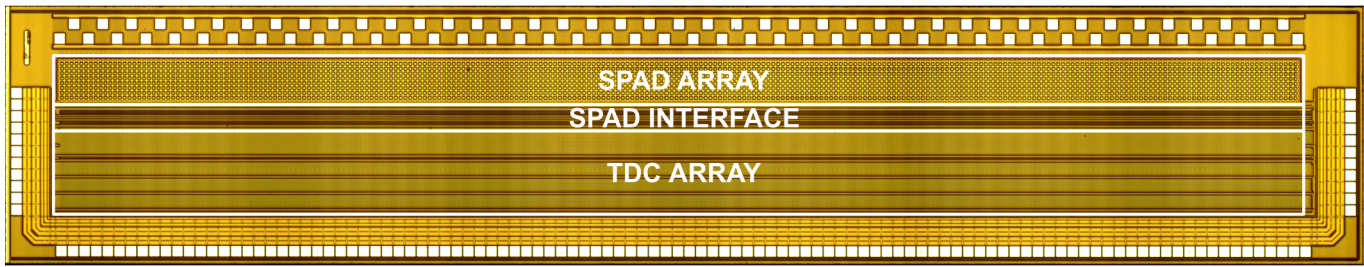
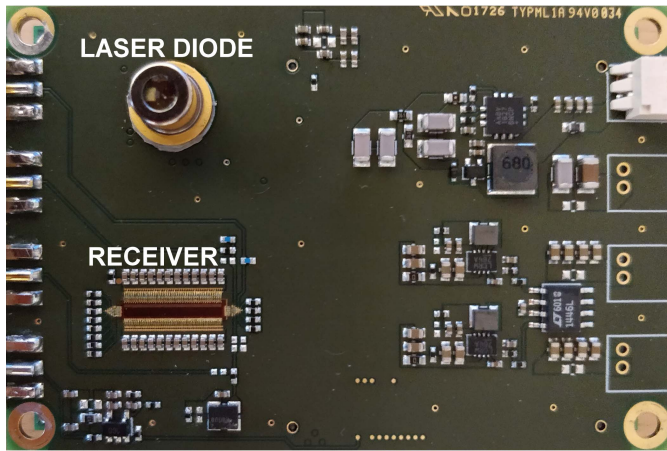


Fig. 8. Photomicrograph of the designed line profiler receiver circuit(11.6mm×2.1mm with pad ring).



(a)



(b)

Fig. 9. Photographs of the designed line profiler PCB and the complete system. (a) Receiver IC and the laser diode on a PCB(7.5cm×5cm). (b) Line profiler with optomechanics.

The linearity of the laser radar was measured at a calibrated measurement track, where it is possible to measure distances up to about 35m. A sheet of brown cardboard with a reflectivity of about 0.7 was used as a target. The distance was increased with a step of 1m and histograms were collected with 5k,10k,20k,40k laser shots accumulated per histogram. Fig. 14 shows the measured nonlinearity of the laser scanner. The peak nonlinearity is about $\pm 2\text{mm}$, however, it is not clear if this error stems from the laser radar electronics or from the track itself.

The standard deviation of the estimated distance was also measured with different number of accumulated laser

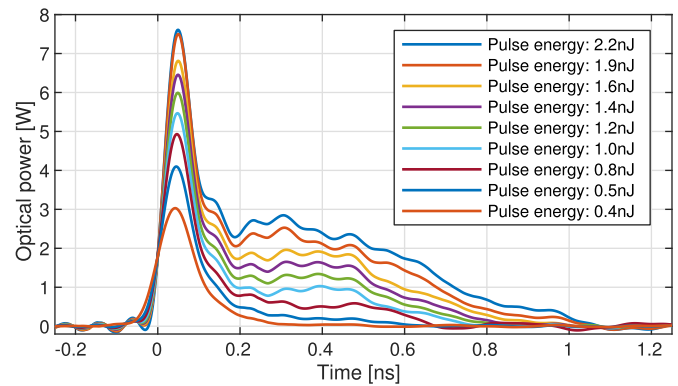


Fig. 10. Optical laser pulse energies and shapes for different drive strengths(measured with a New Focus 1414 25GHz IR photodetector and a 12GHz/40Gsa high speed oscilloscope).

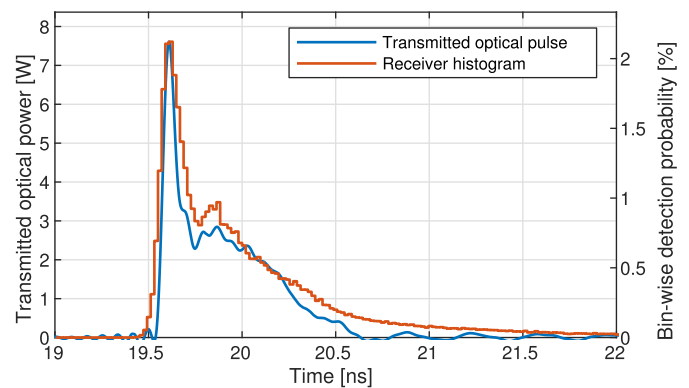


Fig. 11. Receiver detection histogram(target @ 3m) compared to the shape of the real transmitted optical pulse.

shots per histogram. With 5000 shots per frame(i.e. 28fps @ 140kHz pulse rate), the sigma value of the distance is less than 1mm @ 1m. The standard deviation increases linearly with respect to distance, since the power of the received echo is inversely proportional to the square of distance. At 35 meters, the standard deviation @ 28fps is about 1cm.

In general, the standard deviation of ToF measurements is affected by the SPAD jitter, clock jitter, quantization noise of the TDC and the laser pulse width. Because photons are detected within the envelope of the laser pulse, the pulse width directly translates to jitter. If the effects of background detections are neglected for simplicity, the standard deviation

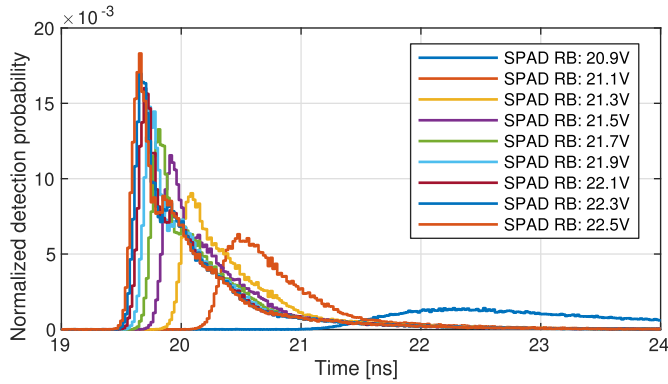


Fig. 12. The effect of SPAD reverse bias to the skew and shape of the histograms.

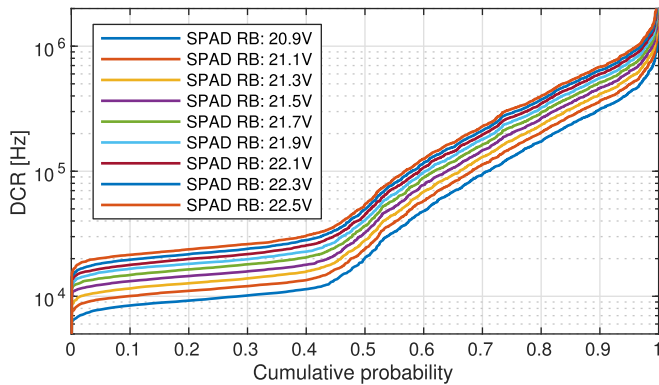


Fig. 13. Cumulative probability distribution of the SPADs' DCR with various reverse bias voltages.

is roughly given by

$$\sigma_{ToF} \approx \sqrt{\frac{\sigma_{SPAD}^2 + \sigma_{TDC}^2 + \sigma_{CLK}^2 + \sigma_{LSR}^2}{N_{det}}}, \quad (8)$$

where σ_{SPAD} , σ_{TDC} , σ_{CLK} are the deviations due to SPAD, TDC and CLK, respectively. σ_{LSR} is the sigma value of the laser pulse, i.e. full-width-half-maximum/2.355 if the pulse is gaussian. N_{det} is the number of detections from the reflected echo. N_{det} is thus proportional to the number of laser shots, energy of the transmitted pulse and to the square of distance. In our case, σ_{LSR} is about 500ps when the tail part of the pulse is also taken into account for which reason the ToF deviation is mainly determined by the pulse width. 500ps sigma for the laser means, for example, that in order to achieve cm-level precision, about 50 detections from the reflected pulse envelope is required.

Fig. 16(a-c) shows an example line profile measured indoors when results from 5000 laser shots are accumulated (i.e. 28fps @ 140kHz pulse rate). The target wall was at a distance of about 16m. No noticeable distortion is present in the measured line profile and all the corners and the large screen are clearly visible.

In outdoor conditions the measurement range is significantly affected by the ambient light level. Since the SPADs are biased above the breakdown voltage at the same time when

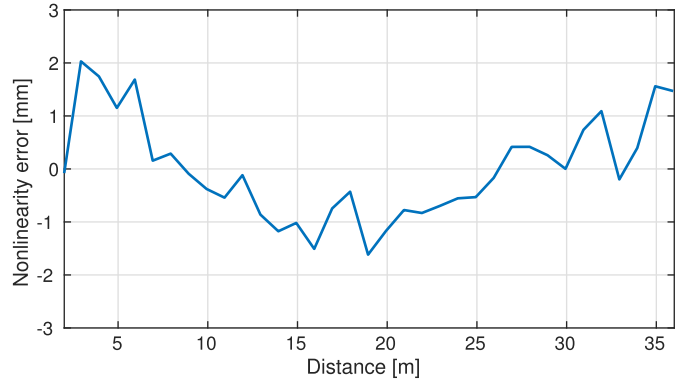


Fig. 14. Accuracy of the line profiler measured indoors at a calibrated linear track with a target reflectance of about 70%.

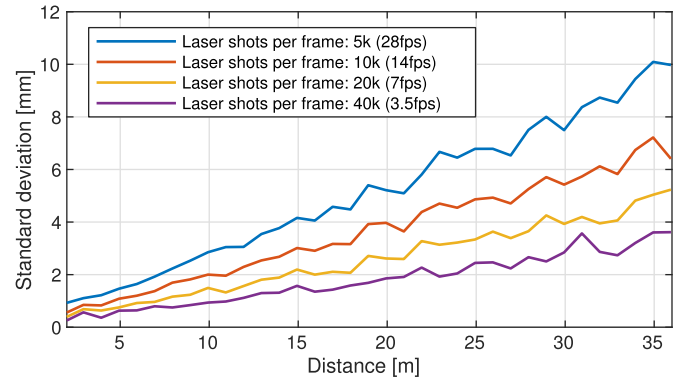


Fig. 15. Standard deviation of the distance results for different amount of accumulated laser shots per frame.

the laser pulse is transmitted, and since the SPADs can be triggered only once per laser shot, the probability to detect a reflected signal photon can be really low when the target is far away. Due to background light, the signal detection probability decreases exponentially with respect to distance as shown in Eqn. (3). In Fig. 2, the expected measurement range of the system is only about 5 meters in high ambient light conditions @ 28fps. However, if the frame rate is lowered and more results are accumulated per histogram, then range can be improved. Fig. 16(d-f) illustrates an extreme case, where results from 12e6 laser shots were accumulated, which allows to detect very weak reflected signals in high ambient light conditions. Signal echoes can be detected even from a distance of 70 meters when enough results are accumulated in the histograms.

Fig. 16f shows a raw data histogram and a normalized and filtered histogram from a single TDC channel (marked as a red point in Fig. 16e), where the optical echo is received from a distance of about 35 meters. From the post-processed histogram it can be seen that the optical power of the received echo is significantly below the ambient light level, being only about 15% of the ambient power impinging the sensor @ 810nm. Using Eqn. (1), and assuming 2nJ of transmitted pulse energy, the average number of received signal photons from 35 meters per pulse can be as low as $10^{-2}..10^{-1}$ depending on the target reflectivity and the angle of incidence. That is, for most of the transmitted pulses, not a single photon is received by the SPAD column. The number of detected signal

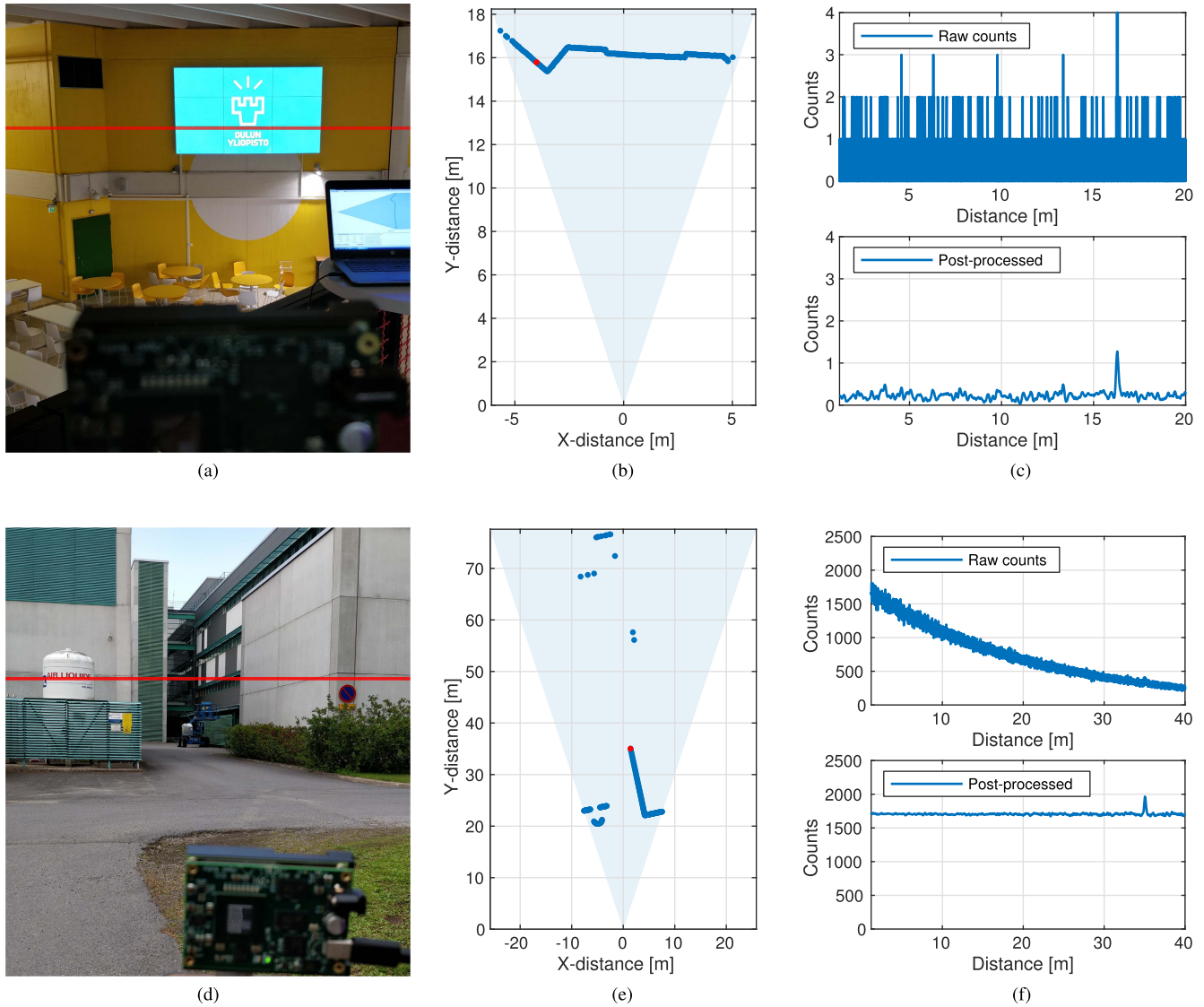


Fig. 16. Example of a line profiles measured indoors and outdoors with 5e3 and 12e6 accumulated laser shots, respectively. (a) Photograph of the indoor setup with an approximate location of the beam. (b) Measured line profile with 5k accumulated laser shots. (c) Raw and processed histograms in low ambient light conditions with a target @ 16 meters. (d) Photograph of the outdoor setup with an approximate location of the beam. (e) Measured line profile with 12M accumulated laser shots. (f) Raw and processed histograms in high ambient light conditions with a target @ 35 meters.

photons is further lowered by the PDP and the blocking effect of the ambient light. From the raw counts shown in Fig. 16f, the sum of background detections up to a distance of 35 meters accounts for 80% of the accumulated laser shots, thus the probability, that the detector is not already blocked before the signal photons arrive from the target, is only 20%. When PDP and blocking is taken into account, the signal detection probability per laser shot can be as low as $10^{-4}..10^{-3}$. However, as shown in the post-processed histogram, even such weak signals are distinguishable when enough results are averaged and the distance can be resolved with cm level precision.

Table I provides a summary of the characteristics of the sensor circuit and the performance of the line profiler system. A comparison against state-of-the-art dToF sensor chips is also provided. However, it should be noted that only [28] presents a line profile receiver system, where also the

field-of-illumination is quite similar to our work. The accuracy and precision are significantly improved in this work even though the system in [28] uses several hundred times more power in illumination. Other previously published works are also listed in the table I, however, comparison is difficult since the systems have different number of pixels, FOV, receiver aperture, illumination power and pulse characteristics, for example. All of these affect the photon detection rates of the signal and background as shown in Eqn. (1) and (2), which makes it complicated to have a meaningful comparison between the systems. For example, [29] uses a 16×1 line receiver, but on the system level the high spatial resolution is achieved through scanning and thus also the illumination differs significantly from other related works. [19] uses a 2-D receiver array to build a full 3-D lidar system. Although the laser pulsing frequency is almost 300 times higher than in our work, the per-pixel illumination power is low due to the larger

TABLE I
SUMMARY OF THE LINE PROFILER

	This work	[28]	[29]	[19]	[21]
Sensor IC characteristics					
Technology	0.35 μ m	0.35 μ m	0.18 μ m	0.18 μ m	0.15 μ m
Pixel array	256 \times 1(8)	80 \times 1(2 \times 2)	16 \times 1(6 \times 4)	252 \times 144	64 \times 64
Pixel pitch [μm]	41.6	50	21	28.5	60
Fill factor [%]	35	19	70	28	26.5
TDC array	256 \times 1	80 \times 1	16 \times 4	144 \times 12	64 \times 64
TDC area [μm²]	30160	16000 ⁽¹⁾	16000 ⁽¹⁾	4200	1800 ⁽¹⁾
TDC resolution [ps]	19.5	312.5	208	48.8	250
TDC depth [bit]	15	12	12	12	16
TDC DNL [LSB]	+0.3/-0.2	N/A	+0.17/-0.17	+0.48/-0.48	+1/-0.8
TDC INL [LSB]	+1/-1.3	N/A	+0.32/-0.56	+0.89/-1.67	+4.8/-3.2
TDC power [mW]	1.6 @ 140ks/s ⁽²⁾	N/A	N/A	0.3	N/A
Lidar system characteristics					
Image resolution	256 \times 1	80 \times 1	202 \times 96(Scanning)	252 \times 144	64 \times 64
Illum. wavelength [nm]	810	905	870	637	470
Mean illum. power [mW]	0.28 @ 140kHz	230 @ 250kHz ⁽⁴⁾	21 @ 133kHz	2 @ 40MHz	N/A
Illum. FOV [°]	37 \times 0.3	40 \times 2	0.05 \times 1.5	40 \times 20	N/A
Frame rate [Hz]	28	N/A	10	30	7.68
Max range [m]	35 @ 28fps	20	100 @ 10fps	0.7 @ 30fps	367 ⁽⁶⁾
Accuracy [mm]	\pm 2	2000	113	88	\pm 1500 ⁽⁶⁾
Precision [mm/%]	10@35m/0.028	500@10m/5	142@100m/0.142	1.4@50m/2.8e-3	200@367m/0.13 ⁽⁶⁾
Power [W]	2.8 ⁽³⁾	1.05 ⁽⁵⁾	6.4	2.54	0.094 ⁽⁵⁾

(1) Estimated from photomicrograph; (2) Includes read-out power; (3) Total system power drawn from USB including also the FPGA development board. (1.8W static power + 1W dynamic power @ 140kHz); (4) Estimated from peak power, pulse width and pulse rate; (5) Receiver IC power only; (6) Emulated performance.

SPAD array and thus the measurement range is limited to less than one meter. [21] also presents a full 3-D lidar system, however its system level performance parameters are based on emulated measurement results.

IV. CONCLUSION

A SPAD based direct time-of-flight receiver sensor for line profiling applications was designed and tested. The receiver, manufactured in 0.35 μ m CMOS technology, consists of 256 columns of SPAD detectors with an independent TDC for each column. The TDCs have a range and resolution of 640ns and 20ps, respectively. Each column has 8 rows of SPADs since biaxial optics arrangement is used. The SPAD pitch is 41.6 μ m and the diameter of the active area is about 25.6 μ m, which gives a fill factor of about 35%. The total chip area is 11.6mm \times 2.1mm(with pad ring), and out of the core area, the SPAD array occupies about 30%, while the rest is taken by the SPAD interface electronics, TDCs and read-out logic.

A demonstrator system with a horizontal FOV of 37° was constructed. With a moderate pulse energy of 2nJ and a repetition rate of 140kHz, the system is capable of very high accuracy and precision and can reliably measure distances up to 30 meters @ 28fps in low ambient light conditions with an accuracy and precision of \pm 2mm and <1cm, respectively. Outdoors, when the target is directly illuminated by the sun, the measurement range @ 28fps is decreased to about

5 meters, however range and precision can be improved at the cost of frame rate.

REFERENCES

- [1] I. Kaisto, J. Kostamovaara, M. Manninen, and R. Myllyla, "Optical range finder for 1.5–10-m distances," *Appl. Opt.*, vol. 22, no. 20, pp. 3258–3264, Oct. 1983.
- [2] R. Schwarte, "Performance capabilities of laser ranging sensors," in *Proc. ESA Workshop Space Laser Appl. Technol.*, May 1984, pp. 61–67.
- [3] G. Kompka, "Optical short-range radar for level control measurement," *IEE Proc. H Microw., Opt. Antennas*, vol. 131, no. 3, pp. 159–164, Jun. 1984.
- [4] J. T. Kostamovaara, K. E. Maatta, and R. A. Myllylae, "Pulsed time-of-flight laser range-finding techniques for industrial applications," *Proc. SPIE*, vol. 1614, pp. 283–295, Mar. 1992.
- [5] S. Donati, *Electro-Optical Instrumentation Sensing and Measuring with Lasers*. Upper Saddle River, NJ, USA: Prentice-Hall, 2004.
- [6] C. Bamji *et al.*, "A 0.13 μ m CMOS system-on-chip for a 512 \times 424 time-of-flight image sensor with multi-frequency photo-demodulation up to 130 MHz and 2 GS/s ADC," *IEEE J. Solid-State Circuits*, vol. 50, no. 1, pp. 303–319, Jan. 2015.
- [7] Y. Kato *et al.*, "320 \times 240 back-illuminated 10- μ m CAPD pixels for high-speed modulation time-of-flight CMOS image sensor," *IEEE J. Solid-State Circuits*, vol. 53, no. 4, pp. 1071–1078, Apr. 2018.
- [8] T.-H. Hsu, T. Liao, N.-A. Lee, and C. C. Hsieh, "A CMOS time-of-flight depth image sensor with in-pixel background light cancellation and phase shifting readout technique," *IEEE J. Solid-State Circuits*, vol. 53, no. 10, pp. 2898–2905, Oct. 2018.
- [9] C. S. Bamji *et al.*, "IMpixel 65nm BSI 320MHz demodulated TOF Image sensor with 3 μ m global shutter pixels and analog binning," in *IEEE Int. Solid-State Circuits Conf. IEEE (ISSCC) Dig. Tech. Papers*, Feb. 2018, pp. 94–96.
- [10] B. Schwarz, "Mapping the world in 3D," *Nature Photon.*, vol. 4, no. 7, pp. 429–430, Jul. 2010.

- [11] Y. Tang *et al.*, "Vision-aided multi-UAV autonomous flocking in GPS-denied environment," *IEEE Trans. Ind. Electron.*, vol. 66, no. 1, pp. 616–626, Jan. 2019.
- [12] R. Halterman and M. Bruch, "Velodyne HDL-64E lidar for unmanned surface vehicle obstacle detection," *Proc. SPIE*, vol. 7692, May 2010, Art. no. 76920D.
- [13] A. Rochas, A. R. Pauchard, P.-A. Besse, D. Pantic, Z. Prijic, and R. S. Popovic, "Low-noise silicon avalanche photodiodes fabricated in conventional CMOS technologies," *IEEE Trans. Electron Devices*, vol. 49, no. 3, pp. 387–394, Mar. 2002.
- [14] M. Perenzoni, L. Pancheri, and D. Stoppa, "Compact SPAD-based pixel architectures for time-resolved image sensors," *Sensors*, vol. 16, no. 5, p. 745, May 2016.
- [15] I. Gyongy *et al.*, "A 256×256, 100-kfps, 61% fill-factor SPAD image sensor for time-resolved microscopy applications," *IEEE Trans. Electron Devices*, vol. 65, no. 2, pp. 547–554, Feb. 2018.
- [16] M. Perenzoni, N. Massari, D. Perenzoni, L. Gasparini, and D. Stoppa, "A 160×120 pixel analog-counting single-photon imager with time-gating and self-referenced column-parallel A/D conversion for fluorescence lifetime imaging," *IEEE J. Solid-State Circuits*, vol. 51, no. 1, pp. 155–167, Jan. 2016.
- [17] D. Bronzi, Y. Zou, F. Villa, S. Tisa, A. Tosi, and F. Zappa, "Automotive three-dimensional vision through a single-photon counting spad camera," *IEEE Trans. Intell. Transp. Syst.*, vol. 17, no. 3, pp. 782–795, Mar. 2016.
- [18] C. Niclass, M. Soga, H. Matsubara, S. Kato, and M. Kagami, "A 100-m range 10-frame/s 340×96-pixel time-of-flight depth sensor in 0.18- μm CMOS," *IEEE J. Solid-State Circuits*, vol. 48, no. 2, pp. 559–572, Feb. 2013.
- [19] C. Zhang, S. Lindner, I. M. Antolović, J. M. Pavia, M. Wolf, and E. Charbon, "A 30-frames/s, 252×144 SPAD flash LiDAR with 1728 dual-clock 48.8-ps TDCs, and pixel-wise integrated histogramming," *IEEE J. Solid-State Circuits*, vol. 54, no. 4, pp. 1137–1151, Apr. 2019.
- [20] I. Vornicu, R. Carmona-Galán, and A. Rodríguez-Vázquez, "Photon counting and direct ToF camera prototype based on CMOS SPADs," in *Proc. IEEE Int. Symp. Circuits Syst. (ISCAS)*, May 2017, pp. 1–4.
- [21] M. Perenzoni, D. Perenzoni, and D. Stoppa, "A 64×64-pixels digital silicon photomultiplier direct tof sensor with 100-mphotons/s/pixel background rejection and imaging/altimeter mode with 0.14% precision up to 6 km for spacecraft navigation and landing," *IEEE J. Solid-State Circuits*, vol. 52, no. 1, pp. 151–160, Jan. 2017.
- [22] J. Kostamovaara *et al.*, "On laser ranging based on high-speed/energy laser diode pulses and single-photon detection techniques," *IEEE Photon. J.*, vol. 7, no. 2, Apr. 2015, Art. no. 7800215.
- [23] J. Huikari, E. Avrutin, B. Ryvkin, and J. Kostamovaara, "High-energy sub-nanosecond optical pulse generation with a semiconductor laser diode for pulsed TOF laser ranging utilizing the single photon detection approach," *Opt. Rev.*, vol. 23, no. 3, pp. 522–528, Jun. 2016.
- [24] J. M. T. Huikari, E. A. Avrutin, B. S. Ryvkin, J. J. Nissinen, and J. T. Kostamovaara, "High-energy picosecond pulse generation by gain switching in asymmetric waveguide structure multiple quantum well lasers," *IEEE J. Sel. Topics Quantum Electron.*, vol. 21, no. 6, pp. 189–194, Nov./Dec. 2015.
- [25] J. J. Degnan, "Photon-counting multikilohertz microlaser altimeters for airborne and spaceborne topographic measurements," *J. Geodyn.*, vol. 34, nos. 3–4, pp. 503–549, Oct. 2002.
- [26] P. Keränen and J. Kostamovaara, "256×TDC array with cyclic interpolators based on calibration-free 2× time amplifier," *IEEE Trans. Circuits Syst. I, Reg. Papers*, vol. 66, no. 2, pp. 524–533, Feb. 2019.
- [27] A. K. Pediredla, A. C. Sankaranarayanan, M. Buttafava, A. Tosi, and A. Veeraraghavan, "Signal processing based pile-up compensation for gated single-photon avalanche diodes," 2018, *arXiv:1806.07437*. [Online]. Available: <https://arxiv.org/abs/1806.07437>
- [28] M. Beer, O. M. Schrey, C. Nitta, W. Brockherde, B. J. Hosticka, and R. Kokozinski, "1×80 pixel SPAD-based flash LIDAR sensor with background rejection based on photon coincidence," in *Proc. IEEE SENSORS*, Oct. 2017, pp. 1–3.
- [29] C. Niclass, M. Soga, H. Matsubara, M. Ogawa, and M. Kagami, "A 0.18- μm CMOS soc for a 100-m-range 10-frame/s 200×96-pixel time-of-flight depth sensor," *IEEE J. Solid-State Circuits*, vol. 49, no. 1, pp. 315–330, Jan. 2014.



Pekka Keränen received the M.Sc. (Tech.) and Dr.Tech. degrees in electrical engineering from the University of Oulu, Finland, in 2010 and 2016, respectively. He is currently a Post-Doctoral Researcher with the Circuits and Systems Research Unit, University of Oulu. His main research interests include integrated circuit design for pulsed time-of-flight laser radars, such as SPAD-based receiver circuits and time-to-digital converters.



Juha Kostamovaara received the Ph.D. degree in electrical engineering from the University of Oulu, Finland, in 1987. He is currently a Full Professor in electronics with the University of Oulu, where he teaches courses on analogue electronics, microelectronics, and optoelectronics. He acted as an Academy Professor nominated by the Academy of Finland from 2006 to 2011 and from 2012 to 2017. He has authored or coauthored more than 450 papers and presentations in international journals and conferences, and holds more than 20 patents, mainly

in the field of optoelectronic sensors. His main research interests include the development of pulsed time-of-flight devices, circuits, and systems for electronic and optoelectronic measurements.